BMC Biology

RESEARCH

Open Access

Genomic and translational insights into eIF2B-mediated salt tolerance in sea rice HD961

Haomin Chen[1,2†], Mingming Chen[1,2,3*†], Shan Yang[1,2†], Hongkai Zhou[1,2,3], Zhihao Xie[1,2], Yongxiang Huang[1,2] and Daming Chen[1,2]

Abstract

Background Soil salinization threatens global rice production, driving the urgent need for salt-tolerant rice cultivars. Sea rice HD961, renowned for its exceptional salt tolerance, serves as an ideal model for elucidating molecular adaptations to salinity.

Results In this study, we generated a high-quality, chromosome-level genome assembly of HD961 using Nanopore long-read sequencing, Illumina short-read polishing, and Hi-C-based scaffolding, providing a robust foundation for translatomic analysis. To explore translational responses to salt stress, we integrated ribosome profiling (Ribo-seq) with the QEZ-seq protocol and RNA sequencing (RNA-seq) under 150 mM NaCl conditions. Our results reveal that salt stress selectively enhances translational efficiency (TE) in genes critical for ion homeostasis, antioxidant defense, and cell wall remodeling, enabling HD961 to maintain cellular balance under stress. Especially, eukaryotic translation initiation factor 2B (eIF2B) emerged as a key regulator, with its upregulation and the formation of stress-induced eIF2B-containing bodies indicating a novel mechanism to optimize protein synthesis. Additionally, ribosome footprint profiling revealed codon-specific modulation of A-site dwell times, with the GCG codon showing a particularly pronounced shift under salt stress, suggesting fine-tuned translational control that prioritizes stress-responsive proteins.

Conclusion Together, these findings highlight eIF2B-mediated translational regulation as central to HD961's salt tolerance, offering valuable genomic and translatomic resources for breeding salt-tolerant rice and other crops.

Keywords Salt stress, eIF2B, Ribosome profiling, Translation regulation, HD961

Background

Rice (*Oryza sativa* L.) is a vital global crop, serving as the primary staple food for over half of the world's population. Its cultivation is crucial for food security and the economic stability of many countries, especially in Asia where rice is deeply embedded in cultural practices and daily life [1–4]. As a model organism, rice possesses a relatively small genome and well-established genetic resources, making it ideal for genetic and genomic studies [5]. Advances in rice genomics have enabled the identification and manipulation of genes responsible for important traits such as yield, disease resistance, and stress tolerance, thereby facilitating the development of

†Haomin Chen, Mingming Chen and Shan Yang contributed equally to this work.

*Correspondence:
Mingming Chen
mingming.chen@gdou.edu.cn
[1] College of Coastal Agricultural Sciences, Guangdong Ocean University, Zhanjiang 524008, China
[2] National Saline-Tolerant Rice Technology Innovation Center, South China, Zhanjiang 524008, China
[3] Shenzhen Institute of Guangdong Ocean University, Shenzhen 518108, China

improved cultivars through both traditional breeding and biotechnological methods [6]. However, despite its significant role, rice production faces increasing threats from various abiotic stresses, with soil salinization emerging as a major and growing concern. Approximately 20% of irrigated lands worldwide are affected by salinity, a figure expected to rise due to factors like sea-level rise, poor irrigation practices, and climate change [7]. High salinity in soil induces osmotic stress, ion toxicity, and nutrient imbalances in rice plants, leading to reduced growth and lower yields [8, 9]. Salt stress particularly impacts critical growth stages such as germination, seedling establishment, and reproductive development, resulting in significant yield losses that threaten food security in affected regions [10–13]. The economic impact is substantial, as vast areas of productive land become unsuitable for cultivation, underscoring the urgent need for strategies to mitigate the effects of salinity on rice crops.

Addressing the challenges posed by saline soils and limited arable land necessitates the development of salt-tolerant rice varieties. While traditional breeding methods have been beneficial, they are often time-consuming and constrained by the complex genetic traits associated with salt tolerance [14]. Therefore, leveraging advanced genomic and molecular tools is crucial to accelerate the identification of key genes and regulatory networks that confer salt tolerance [10]. Salt-tolerant rice varieties can stabilize and potentially increase yields in saline environments, expand cultivation areas, and enhance food security and economic resilience [14]. Moreover, understanding salt tolerance mechanisms in rice can inform efforts to improve abiotic stress resilience in other staple crops, thereby having a broader impact on global agriculture. Salt tolerance in rice involves intricate physiological and molecular responses, including gene regulatory networks, signal transduction pathways, and metabolic adjustments that enhance ion homeostasis, osmoprotection, and oxidative stress mitigation [15]. To unravel these complexities, comprehensive genomic and translatomic analyses are essential. Genome sequencing provides a foundational understanding, enabling the identification of genetic variants, gene families, and regulatory elements linked to salt tolerance [16–18]. However, transcriptomic data alone may not capture the dynamic changes in protein synthesis that are crucial for adaptive responses to salinity [19].

To bridge this gap, translatomics, particularly ribosome profiling (Ribo-seq), offers a detailed view of translation by mapping ribosome-protected mRNA fragments (RPFs) and measuring translational efficiency (TE) across the genome [20–23]. When combined with RNA sequencing (RNA-seq), Ribo-seq allows for the analysis of translational control mechanisms, revealing how plants adjust protein synthesis in response to environmental stresses [20–22, 24, 25]. This integrated approach is essential for identifying not only differentially expressed genes but also those with altered translational regulation, providing a deeper understanding of the molecular strategies used by salt-tolerant cultivars like HD961. Recent advancements in sequencing technologies have greatly enhanced the ability to generate high-quality genomic and translatomic data. Long-read sequencing platforms, such as Oxford Nanopore Technologies and Pacific Biosciences, enable the assembly of highly contiguous and accurate genome sequences by spanning repetitive regions and resolving structural variants that are difficult to detect with short-read technologies [26, 27]. Combining long-read sequencing with short-read sequencing for error correction and polishing results in chromosome-level genome assemblies necessary for comprehensive gene annotation and functional genomics studies. Additionally, Hi-C–based scaffolding utilizes chromatin interaction data to organize contigs into chromosome-scale assemblies, achieving exceptional genome completeness and accuracy [28]. Concurrently, the development of robust ribosome profiling protocols, like QEZ-seq, has improved the quality and reliability of Ribo-seq data, ensuring accurate mapping of RPFs and precise estimation of TE [29]. These technological innovations enable researchers to perform integrative analyses that link genome structure with functional proteomics, elucidating the molecular basis of complex traits such as salt tolerance.

Plant stress adaptation increasingly hinges on control at the translation level, distinct from well-studied transcriptional changes [30]. Under salt stress, plants globally slow protein synthesis while selectively boosting the translation of crucial stress-response proteins (e.g., ion transporters, osmoprotectants, antioxidants) to survive high salinity [10, 31, 32]. This translational reprogramming is mediated by changes in ribosome occupancy and initiation factor activity that prioritize essential mRNAs. For example, salt and other stresses activate kinases that phosphorylate eukaryotic initiation factor 2 (eIF2), causing it to bind its guanine nucleotide exchange factor eIF2B and stall general translation initiation [30]. This conserves energy but permits preferential synthesis of defense proteins via selective mRNA translation. In parallel, plants modulate specific translation factors to fine-tune protein production. The RNA helicase eIF4A needed for ribosome scanning is tightly regulated under salinity to ensure rapid translation of stress-protective proteins without wasteful activity. For example, partially dampening eIF4A can increase stress tolerance: an RNA aptamer that binds and modestly inhibits eIF4A's cap-dependent initiation activity conferred enhanced salt

tolerance in rice, improving growth and photosynthesis under high salt [33]. Likewise, targeting the elongation phase has yielded benefits—stabilizing the essential elongation factor eEF1A with a specific RNA aptamer preserved overall translation under salt stress and bolstered rice salt tolerance [34]. Consistently, transgenic plants overexpressing eEF1A1 show increased salinity tolerance (e.g., better root growth and less oxidative damage) compared to wild types [32]. Such findings underscore that chemical or genetic modulation of translation components can reprogram stress outcomes: for instance, exogenous polyamines like spermidine have been shown to enhance salt resilience, apparently by promoting translation of stress-protective proteins and antioxidant enzymes [9]. Together, these advances reveal translational control by regulated initiation, selective ribosome engagement, and elongation efficiency, which is a critical layer of salt-stress adaptation independent of transcriptional changes. Indeed, the recent identification of eIF2B as a salt-responsive translational regulator adds a new dimension to our understanding, spotlighting the translation machinery itself as a promising target for engineering salt-resilient crops [35].

HD961 is an exemplary model for studying salt tolerance in rice due to its remarkable resilience in high-salinity environments. Originating from coastal saline soils, HD961 demonstrates superior growth and yield stability under salt stress compared to conventional cultivars [36, 37]. Preliminary studies have identified numerous candidate genes involved in ion transport, antioxidant defense, and cell wall remodeling that contribute to HD961's adaptive traits. However, a comprehensive understanding of the genomic and translational mechanisms driving HD961's salt tolerance requires a detailed chromosome-level genome assembly and translatomic profiling. In this study, we present a high-quality, chromosome-level genome assembly of HD961, achieved through the integration of Nanopore long-read sequencing, Illumina short-read polishing, and Hi-C–based scaffolding. Building on this genomic foundation, we utilize ribosome profiling (Ribo-seq) with the QEZ-seq protocol alongside RNA sequencing (RNA-seq) to investigate the translational dynamics underlying HD961's salt tolerance [20–22]. By identifying genes with altered TE and analyzing codon-specific ribosome stalling events, we aim to uncover the post-transcriptional regulatory mechanisms that enable adaptive protein synthesis in response to salinity stress. This comprehensive approach not only enhances our understanding of salt tolerance in rice but also provides valuable genomic and translatomic resources for future breeding and biotechnological efforts to improve abiotic stress resilience in crops.

Results

HD961 genome assembly and annotation

We assembled a 426.53 Mb genome with a contig N50 of 6.27 Mb using Nanopore long-read sequencing data, achieving a robust assembly post Illumina short-read polishing and Hi-C-based scaffolding with a scaffold N50 of 33.16 Mb (Additional file 1: Table S1). We evaluated the completeness of the genome assembly using two widely recognized methods: CEGMA (Core Eukaryotic Genes Mapping Approach) and BUSCO (Benchmarking Universal Single-Copy Orthologs). CEGMA analysis showed that 454 (99.13%) of the 458 core eukaryotic genes were detected, including 238 (95.97%) of the 248 highly conserved genes. Meanwhile, BUSCO analysis revealed that 3039 (93.91%) of the 3236 universal single-copy orthologs were complete, with 2953 (91.25%) classified as single-copy and 86 (2.66%) considered duplicated. Only 102 (3.15%) were fragmented and 95 (2.94%) were missing. Overall, both CEGMA and BUSCO demonstrate a high level of completeness, indicating that the assembly successfully captures the vast majority of essential eukaryotic genes (Tables 1 and 2).

After Hi-C–based scaffolding (Table 3), the genome assembly was anchored into 85 scaffolds with a total length of 426.55 Mb. The scaffold N50, which measures the size above which half of the total assembly length is contained, reached 33.16 Mb, and the longest single scaffold was 45.65 Mb. At the contig level, 272 contigs were identified, collectively measuring 426.53 Mb, with a contig N50 of 4.80 Mb and a maximum contig length of 22.09 Mb. The assembly shows an overall GC content of 43.83%. Notably, gaps are minimal: only 187 gaps were detected, totaling 18,700 bp in length, highlighting the high contiguity and completeness of the

Table 1 CEGMA completeness metrics for the genome assembly

Number of 458 CEG* present in assembly	%of 458 CEGs present in assemblies	Number of 248 highly conserved CEGs present	% of 248 highly conserved CEGs present
454	99.13%	238	95.97%

Note: CEG* refers to Core Eukaryotic Genes as defined in the CEGMA v2.5 database

Table 2 BUSCO evaluation results for the genome assembly

Complete BUSCOs(C)	Complete and single-copy BUSCOs(S)	Complete and duplicated BUSCOs(D)	Fragmented BUSCOs(F)	Missing BUSCOs(M)	Total lineage BUSCOs
3039 (93.91%)	2953 (91.25%)	86 (2.66%)	102 (3.15%)	95 (2.94%)	3236

Table 3 Genome assembly statistics after Hi-C scaffolding

TotalNum	MinLen	ScfNum	ScfLen	ScfN50	ScfN90	ScfMax	mScfNum	mScfLen
85	1,000	85	426,553,376	33,163,565	26,782,549	45,654,565	0	0
CtgNum	CtgLen	CtgN50	CtgN90	CtgMax	GC(%)	GapNum	GapLen	MaxGap
272	426,534,676	4,804,654	894,622	22,095,263	43.83	187	18,700	100

assembly. In parallel, transposable element (TE) analysis (Fig. 1A, Table 4) reveals that TEs occupy a substantial portion of the genome. Class I retrotransposons (e.g., LTR/Gypsy and LTR/Copia) comprise 43,399 elements spanning 99.62 Mb (23.35% of the genome), while Class II DNA transposons encompass 126,340 elements totaling 50.43 Mb (11.82%). Within Class II, CACTA elements make up one of the largest fractions. Overall, these findings underscore the robust quality of the Hi-C–assembled genome and the considerable contribution of TEs to its repetitive landscape.

Gene prediction and functional annotation

Integrating ab initio, homology-based, and transcript-based gene prediction approaches, we identified a total of 39,565 protein-coding genes in the HD961 genome (Additional file 1: Table S2). The predicted genes have an average length of approximately 2.89 kb and consist of an average of 4.43 exons per gene, indicative of a compact gene structure typical of rice (Additional file 2: Fig. S1A). Detailed analyses of the gene architecture shows the distribution of gene lengths and exon counts across the genome (Fig. 1B, C). Clean RNA-seq data were also aligned to the assembled genome using HISAT2. We then quantified the mapping across exonic, intronic, and intergenic regions. Notably, 91.94% of the reads mapped to annotated exons, which strongly supports the accuracy and completeness of our gene prediction model (Fig. 1D). For functional characterization, the predicted protein-coding genes were extensively annotated against multiple databases, including NR, SwissProt, TrEMBL, Pfam, eggNOG, GO, and KEGG. As demonstrated in Fig. 2, approximately 95.64% of the predicted genes could be functionally characterized, with 70.8% of these genes assigned to Gene ontology (GO) categories. KEGG pathway mapping showed that 61.7% of the genes are associated with metabolic and signaling pathways that facilitate environmental stress adaptation. Furthermore, GO annotation revealed that a significant proportion of genes are involved in key biological processes, such as ion transport, signal transduction, and stress response, which are critical for salt stress defense (Fig. 1E). In HD961 (Fig. 1F), the scaffold N50 of 33.16 Mb matches the high contiguity of other top-tier rice assemblies as R498 [38], IR64 [39], and Nipponbare [40]. The 93.9% BUSCO completeness confirms that nearly all core plant genes are present. As shown in Fig. 1G, HD961 harbors 39 565 predicted protein-coding genes, comparable to Nipponbare and R498, with an average transcript length of ~ 2.89 kb and 4.43 exons per gene, reflecting a conserved gene architecture across *O. sativa* cultivars. The transposable-element landscape of HD961 (Fig. 1H) is likewise typical of indica genomes, with LTR/Gypsy elements comprising 16.1% of the assembly, DNA transposons 11.8%, LTR/Copia 2.7%, and the remainder in other TE families. Together, these comparisons demonstrate that HD961's genome assembly quality and overall structural features are on par with, and in some respects subtly distinct from, established reference genomes, supporting its utility for downstream functional and comparative analyses. The distribution of genes across diverse metabolic pathways demonstrated the enrichment of pathways such as TCA cycle (Additional file 2: Fig. S1B).

In addition to protein-coding gene annotation, our analysis revealed a diverse noncoding RNA (ncRNA) landscape within the HD961 genome. We identified 918 tRNAs, 464 rRNAs, 195 miRNAs, and a total of 744 snRNAs/snoRNAs (including 91 snRNAs and 653 snoRNAs), highlighting their potential roles in post-transcriptional regulation and stress responses (Fig. 2A). The abundance of snoRNAs and tRNAs suggests active regulatory functions in maintaining cellular homeostasis under salt stress. Furthermore, our genome-wide analysis predicted the presence of 325 pseudogenes across the genome (Fig. 2B). These pseudogenes, which likely arose due to frameshift mutations or premature stop codons in duplicated gene families, may serve as reservoirs for evolutionary innovation or regulatory elements influencing gene expression networks. The total length of pseudogenes spans a significant portion of the genome, with an average length indicative of evolutionary conservation and functionality. To gain insight into the chromosomal distribution and organization, we visualized the annotated features of the HD961 genome across its 12 chromosomes (Fig. 2C). The representation highlights gene-rich regions and repetitive elements, providing a comprehensive overview of the structural complexity of the genome. In addition, Hi-C contact map analysis provided a high-resolution view of the genome's three-dimensional organization (Fig. 2D). The strong diagonal

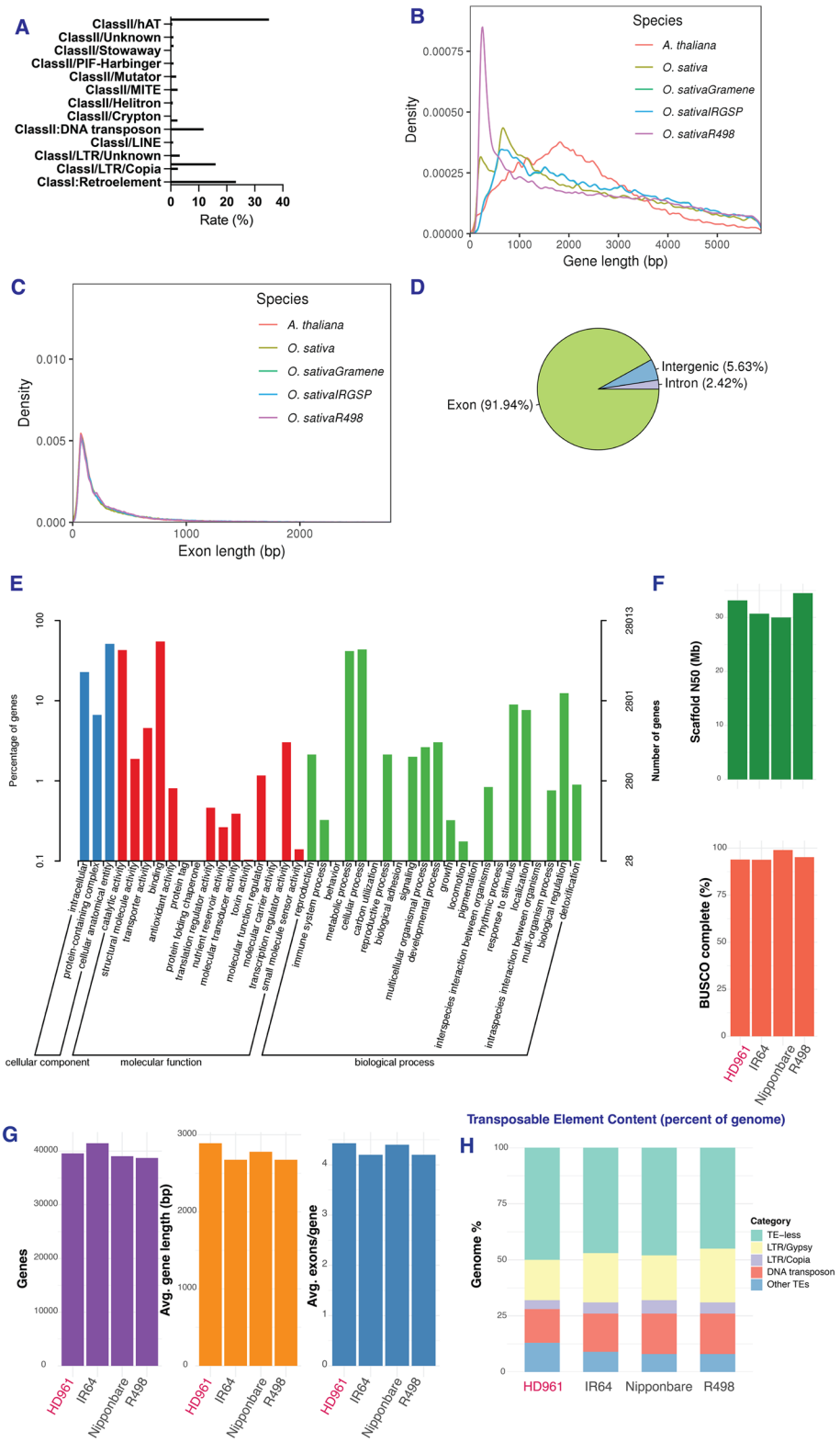

Fig. 1 Comprehensive Landscape of HD961 Genome. **A** Relative proportions of Class I and Class II TE superfamilies. **B** Size distribution profiles for each major TE class. **C** Copy-number distributions as a function of TE length; **D** Whole-genome fraction occupied by each TE category. **E** Functional annotation of genes neighboring TE insertions, highlighting enriched pathways and gene families. **F** Scaffold N50 and BUSCO completeness for HD961 versus published rice genomes. **G** Protein-coding gene count, average gene length, and average exons per gene in HD961 compared with Nipponbare and R498. **H** Proportional composition of major transposable-element classes in HD961 and reference rice genomes

Table 4 Summary of transposable element (TE) sequences in the genome assembly

Type	Number	Length	Rate (%)
ClassI:Retroelement	43,399	99,615,047	23.35
ClassI/LTR/Cassandra	5	312	0.00
ClassI/LTR/Caulimovirus	64	238,874	0.06
ClassI/LTR/Copia	4353	11,344,914	2.66
ClassI/LTR/Gypsy	14,276	68,696,589	16.11
ClassI/LTR/Pao	354	54,020	0.01
ClassI/LTR/Unknown	12,989	14,164,484	3.32
ClassI/LTR/Viper	13	2644	0.00
ClassI/DIRS	295	16,981	0.00
ClassI/LINE	6185	4,216,501	0.99
ClassI/LTR/ERV	2209	246,453	0.06
ClassI/SINE	2656	633,275	0.15
ClassII:DNA transposon	126,340	50,433,520	11.82
ClassII/Academ	31	2292	0.00
ClassII/CACTA	7150	10,820,584	2.54
ClassII/Crypton	243	20,945	0.00
ClassII/Dada	85	52,883	0.01
ClassII/Ginger	132	11,700	0.00
ClassII/Helitron	3678	3,170,223	0.74
ClassII/IS3EU	101	8021	0.00
ClassII/Kolobok	82	56,461	0.01
ClassII/MITE	43,031	11,050,131	2.59
ClassII/Maverick	213	15,730	0.00
ClassII/Merlin	38	2293	0.00
ClassII/Mutator	14,259	8,784,749	2.06
ClassII/Novosib	140	9,019	0.00
ClassII/P	129	10,759	0.00
ClassII/PIF-Harbinger	16,329	4,739,627	1.11
ClassII/PiggyBac	477	216,781	0.05
ClassII/Sola	113	9890	0.00
ClassII/Stowaway	29	1734	0.00
ClassII/Tc1-Mariner	21,015	4,786,108	1.12
ClassII/Tourist	95	12,437	0.00
ClassII/Unknown	13,853	4,480,471	1.05
ClassII/Zator	9	443	0.00
ClassII/Zisupton	145	15,288	0.00
ClassII/hAT	4963	2,154,951	0.51
Total	169,739	150,048,567	35.18

signal observed in the Hi-C contact matrix indicates well-anchored chromosomal interactions, confirming the high contiguity and accuracy of our genome assembly. The Hi-C scaffolding approach successfully anchored the majority of assembled contigs into chromosome-scale scaffolds, enhancing our understanding of the spatial architecture of the HD961 genome. In addition, HD961 displays the greatest number of large structural variants relative to Nipponbare with approximately 25,000 insertions and deletions, while IR64 and R498 harbor progressively fewer (~20,000 and ~15,000 SVs, respectively) (Fig. 2E). In contrast, copy-number analysis of five major salt-tolerance gene families shows identical counts across all three indica lines: a single HKT1;5 locus; ~35 LEA genes; ~32 ROS-scavenging enzymes; ~90 bZIP transcription factors; and ~130 MYB transcription factors (Fig. 2F). These results indicate that HD961's enhanced salt resilience does not arise from wholesale gene-family expansion or a higher TE/SV load in known stress genes, but rather from specific allelic variants or regulatory changes within these conserved loci. Collectively, these findings demonstrate the robustness of our genome annotation strategy, providing valuable insights into the regulatory and structural components that contribute to HD961's remarkable salt tolerance.

Quality assessment of ribosome-protected footprints

To investigate the translatome landscape of sea rice HD961 under salt stress, we performed ribosome profiling (Ribo-Seq) using the QEZ-seq protocol on HD961 root tissues exposed to 150 mM NaCl treatment (Fig. 3A). The quality of the sequencing reads was assessed using multiple key metrics to ensure data reliability and precision. First, the read length distribution analysis confirmed that the majority of ribosome-protected fragments (RPFs) fell within the expected 27–30 nt range, characteristic of actively translating ribosomes (Fig. 3B). This distribution ensures the accurate capture of ribosome footprints, supporting the integrity of the sequencing data. Ribo-Seq libraries yielded on average 5.34 million input reads of 37 nt, with 3.58 million (≈26.3%) uniquely mapping to the HD961 assembly and an average aligned length of 26.5 nt (Additional file 1: Table S3). Splice junction analysis detected 45,388 total splicing events with predominantly GT/AG (66.4%), followed by GC/AG (5.7%) and AT/AC (0.6%), confirming robust coverage across exon–intron boundaries. Base-calling accuracy was high, with mismatch, insertion, and deletion rates of 0.80%, 0.02%, and 0.03%, respectively, and only 15.6% of reads mapping to multiple loci. Unmapped reads were almost entirely due to excessive mismatches (2.46 million; 0.09%) rather than read length, and chimeric reads were negligible ($n = 8$). Together, these metrics demonstrate the high quality and specificity of our Ribo-seq data for downstream translational analyses. The analysis of read extremities further validated the data quality by showing a strong 3-nt periodicity at both the 5′ and 3′ ends of the reads (Fig. 3C). This periodicity is a hallmark of efficient translation, indicating that ribosomes are properly engaged with mRNAs and elongation is

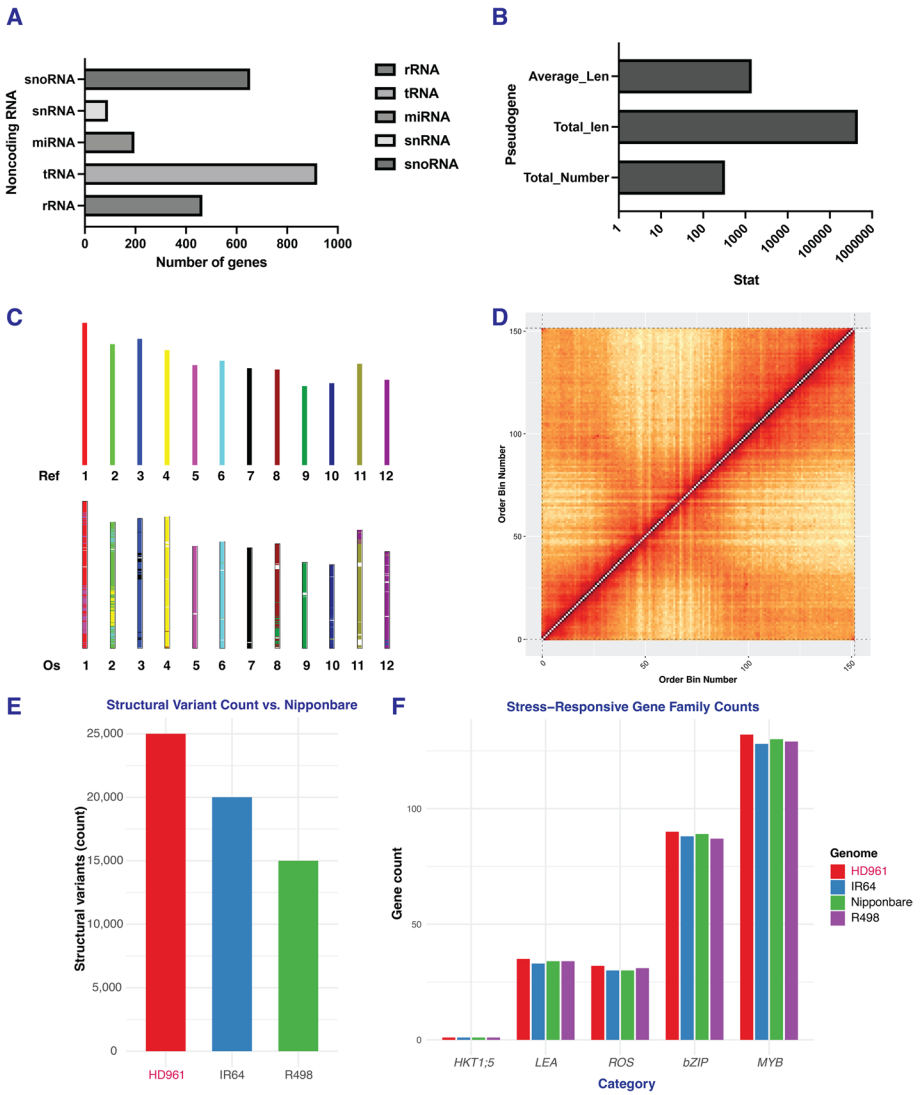

Fig. 2 Comprehensive analysis of noncoding RNAs, pseudogenes, chromosomal organization, and Hi-C genome assembly in sea rice HD961. **A** Noncoding RNA distribution. **B** Pseudogene statistics. **C** Chromosomal organization. **D** Hi-C genome assembly. **E** Counts of large structural variants in HD961, IR64, and R498 relative to the Nipponbare reference genome. **F** Copy numbers of key salt-tolerance gene families (*HKT1;5*, LEA proteins, ROS-scavenging enzymes, bZIP, and MYB transcription factors) in HD961, IR64, and R498

occurring in a coordinated manner under salt stress conditions. Metagene analysis of ribosome P-site occupancy relative to start and stop codons revealed distinct peaks at these regions (Fig. 3D), highlighting efficient ribosomal pausing and translation regulation. To further confirm the robustness of our genome assembly, we performed a parallel analysis by mapping the RPFs to the Nipponbare reference genome (Additional file 2: Fig. S2). The quality metrics obtained from the Nipponbare reference showed a similar read length distribution pattern (Additional file 2: Fig. S2A), with RPFs primarily ranging within the 27–32 nt region. The periodicity observed in the read extremities (Additional file 2: Fig. S2B) displayed consistent patterns with our assembled genome, further demonstrating the high quality of the HD961 assembly. The metagene analysis for Nipponbare (Additional file 2: Fig. S2C) also indicated strong P-site accumulation at translation start and stop codons, reinforcing the reliability of both reference genomes. Ribo-seq and RNA-seq libraries displayed high within-method reproducibility, with Pearson's $r \geq 0.90$ between biological replicates in both CK and salt-stressed samples (Additional file 2: Fig. S2D). Cross-platform correlations were modest ($r \approx 0.50–0.60$), reflecting the different layers of regulation captured by Ribo-seq versus RNA-seq (Additional

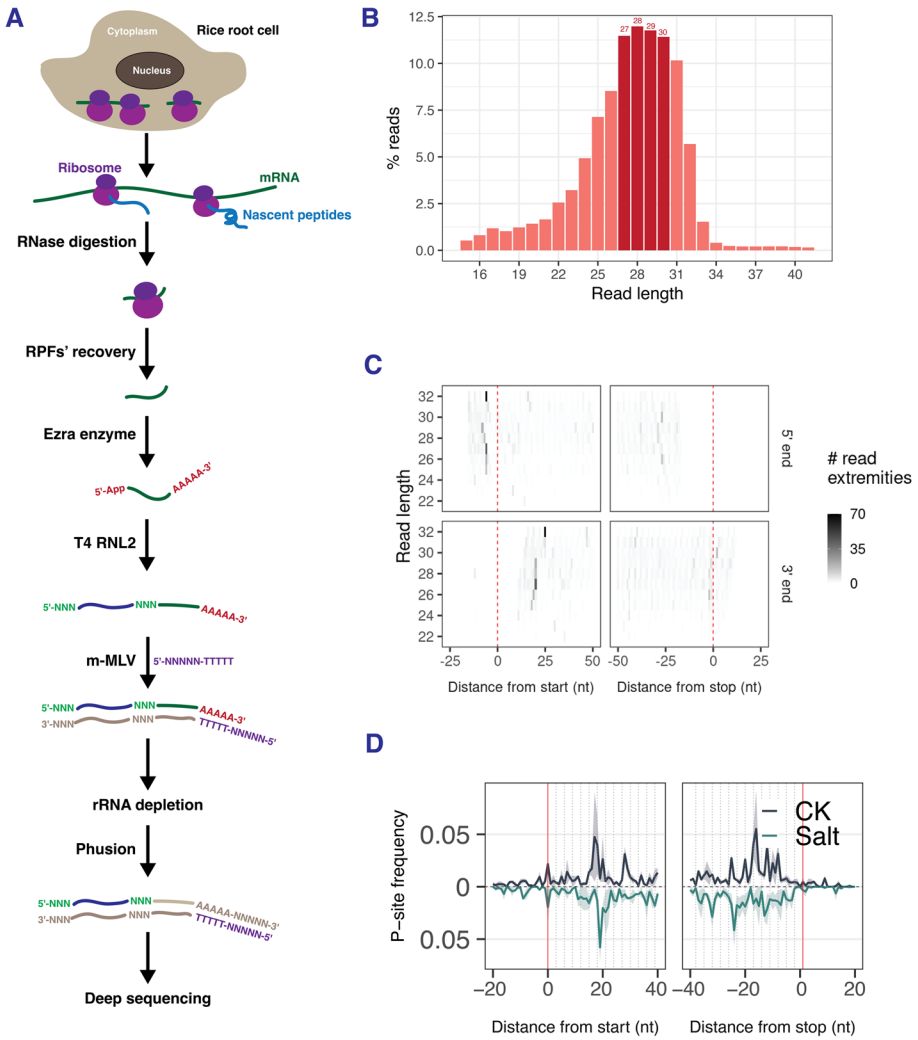

Fig. 3 QEZ ribosome profiling workflow and quality assessment in sea rice HD961. **A** Ribosome profiling workflow showing key steps from RNA extraction to deep sequencing. **B** Distribution of ribosome-protected fragment (RPF) read lengths highlighting 27-30nt with dark red. **C** Distribution of read extremities relative to the start and stop codons. **D** P-site frequency plot showing ribosome positioning around the start and stop codons

file 2: Fig. S2D). Ribo-seq replicates under salt stress correlated slightly better with each other ($r = 0.90$–1.00) than with control samples ($r = 0.75$–0.79), indicating a consistent translational response to salinity. Together, these data confirm library quality and support the interpretation of differential expression and translational efficiency analyses. The comparable quality of ribosome footprint data mapped to our HD961 assembly and the Nipponbare reference underscores the accuracy and completeness of the de novo assembled HD961 genome. The well-maintained periodicity, codon-specific ribosome occupancy, and P-site enrichment in both datasets confirm that our assembly provides a robust framework for translational analysis. These results affirm that the HD961 genome assembly is of high quality, comparable to the well-established Nipponbare reference, and is suitable for further exploration of translational efficiency and stress adaptation mechanisms in sea rice HD961.

Translational dynamics in sea rice HD961 under salt stress

To investigate translational dynamics in sea rice HD961 under control (CK) and salt-stress conditions, we analyzed ribosome P-site distribution across different transcript regions (Fig. 4A). The results indicate that translation predominantly occurs within the coding sequences (CDS), with a strong preference for frame 0, suggesting robust translation through canonical open reading frames. The distribution of P-sites in the 5′ and 3′ untranslated regions (UTRs) remains relatively low under

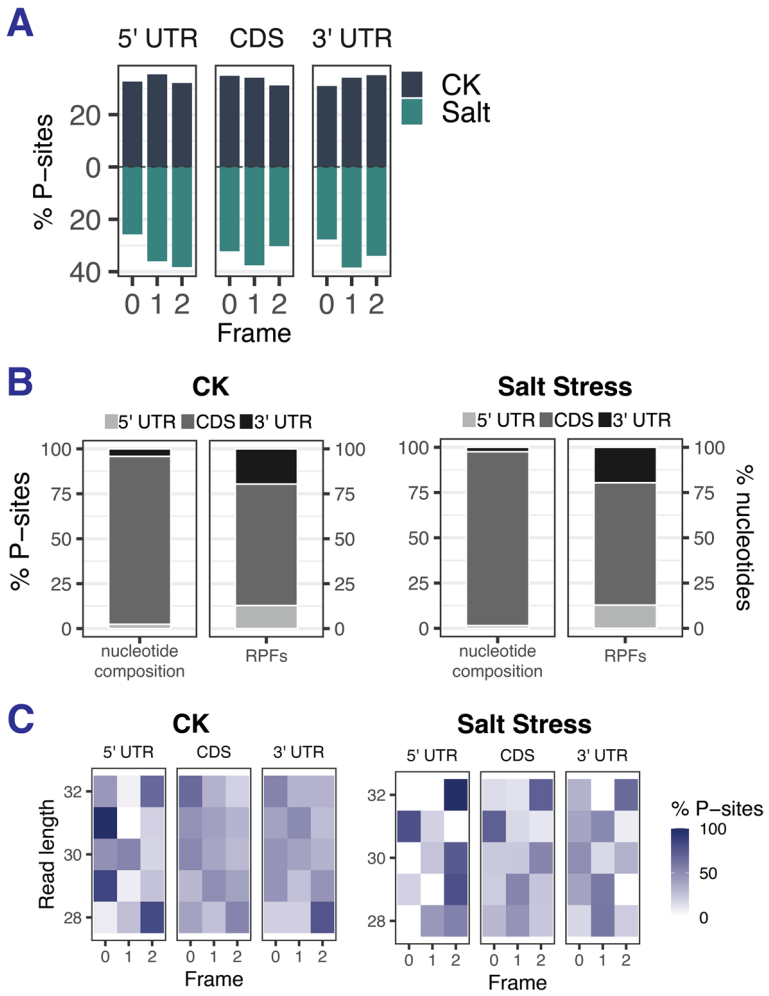

Fig. 4 Ribosome P-site distribution and translational dynamics in sea rice HD961 under salt stress. **A** Frame distribution across transcript regions. **B** Comparison of transcript nucleotide composition and RPFs across 5′UTR, CDS, and 3′ UTR. **C** Ribosome positioning around start and stop codons

both conditions, reinforcing their limited contribution to active translation. Despite the presence of salt stress, the overall translational landscape appears stable, with consistent ribosome positioning across the transcriptome. A comparison of the proportion of P-sites relative to the transcript length (Fig. 4B) further highlights the dominance of the CDS in translational activity. The data suggest that, even under salt stress, the majority of ribosome footprints are concentrated within coding regions, while the 5′ and 3′ UTRs show fewer P-sites than their respective nucleotide lengths would predict. This pattern underscores the prioritization of protein-coding regions in maintaining translational efficiency during stress adaptation. An analysis of ribosome positioning relative to the start and stop codons (Fig. 4C) reveals distinct peaks under both CK and salt stress conditions, indicative of efficient translation initiation and termination. The consistent ribosome occupancy at these critical sites suggests that the core translational machinery remains largely unaffected by salt stress, ensuring the continued synthesis of essential proteins necessary for stress adaptation. To further evaluate the translational response, we compared the mapping results to the Nipponbare reference genome (Additional file 2: Fig. S3). While the overall patterns of P-site distribution were similar, subtle differences were observed in the relative distribution of P-sites across transcript regions (Additional file 2: Fig. S3A). Mapping to the HD961 genome provided a more refined view of translational activity, with stronger signals observed in the CDS and clearer periodicity patterns. In contrast, the Nipponbare reference showed a slightly broader distribution of P-sites, which may reflect differences in genome annotation or structural variations between the two genomes (Additional file 2: Fig. S3B, C). These findings (Fig. 4, Additional file 2: Fig. S3) suggest that while the core translational processes are well-conserved, the

choice of reference genome can influence the resolution of translational insights. The high-quality mapping to the HD961 assembly confirms its suitability for studying translational regulation, providing a comprehensive framework for understanding how HD961 adapts to salt stress at the translational level.

Codon usage profiling at the E, P, and A sites in sea rice HD961 under salt stress

We investigated codon usage patterns at the E, P, and A sites of ribosomes in sea rice HD961 under control (CK) and salt-stress conditions. As illustrated in Fig. 5A, ribosome occupancy differed across codons, with start codons (blue) and stop codons (red) showing distinct usage patterns, emphasizing their essential roles in translation initiation and termination. Most codons within the middle of the coding sequences (CDS) exhibited high usage indices, suggesting a preference for these codons, whereas codons near the 3′ end of the CDS had lower usage, indicative of slower ribosomal movement (Additional file 2: Fig. S4A). While overall codon usage remained largely consistent between conditions, subtle changes were observed under salt stress, as shown in Fig. 5B. These slight modifications in codon

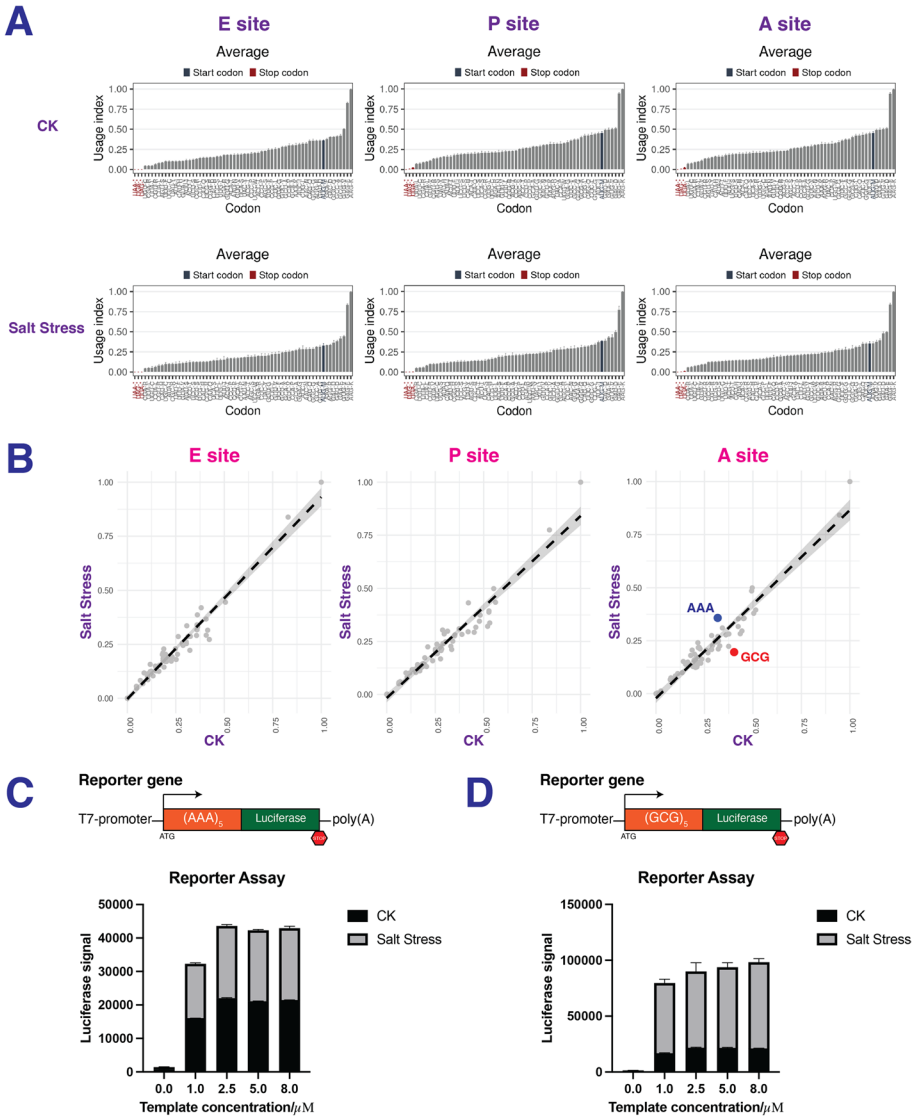

Fig. 5 Codon usage profiles at the E, P, and A sites in sea rice HD961 under control and salt stress. **A** Codon usage patterns at the E, P, and A sites in ribosomes for control (CK) and salt-stress conditions, showing the usage index for each codon across the translation process. **B** Scatter plots showing the correlation of codon usage at the E, P, and A sites between control and salt-stressed conditions, highlighting the consistency of usage patterns with slight shifts under stress. **C** Reporter assay of $(AAA)_5$-driven translation under control (CK) and salt stress. **D** Reporter assay of $(GCG)_5$-driven translation under control (CK) and salt stress. Values are presented as the mean ± standard deviation ($n = 3$)

usage at the E, P, and A sites imply that salt stress triggers translational fine-tuning, optimizing protein synthesis to cope with environmental challenges. At the A site, two codons—AAA and GCG—stood out as outliers in the correlation analysis, prompting us to design a reporter to explore their roles in translational adjustments (Fig. 5C, D). Consequently, the reporter with GCG codons exhibited increased translational signals under salt stress, suggesting reduced occupancy at the A site (Fig. 5D), while the AAA codon showed no significant changes (Fig. 5C). Additionally, transcripts whose translation efficiency increases under salt stress have the lowest GCG codon occupancy at the ribosome A site, those whose translation efficiency decreases have intermediate occupancy, and transcripts with no change carry the highest occupancy (Additional file 2: Fig. S4B), indicating that codon position and GCG stalling correlate with changes in translation efficiency under salt stress. These findings indicate that sea rice HD961 may employ an adaptive strategy at the A site to sustain protein synthesis under stress, contributing to its resilience in saline environments.

eIF2B is a key regulator in salt stress adaptation of sea rice HD961

Building on above codon-level observations, we explored broader regulatory mechanisms governing translation under salt stress. Gene ontology (GO) enrichment analysis of differentially expressed genes (DEGs) associated with translation efficiency in sea rice 86 (HD961) under salt stress (150 mM NaCl) highlighted the importance of translation regulation in the plant's response to salt stress. The analysis revealed that genes related to translation machinery, including those involved in protein transport, protein phosphorylation, nucleotide binding, GTP binding, and RNA binding, were significantly upregulated (highlighted in magenta in Additional file 2: Fig. S4A). This indicates that translation regulation plays a central role in HD961's adaptation to high salt conditions, likely through enhanced protein synthesis mechanisms to cope with the stress environment. Within this context, eIF2B, a key translation factor involved in translation initiation and ribosome biogenesis, was identified as a major regulator of translation under salt stress. Differential gene expression analysis revealed a marked upregulation of eIF2B in salt-stressed HD961 (Fig. 6A), underscoring its critical role in managing the increased demand for protein synthesis during stress. The upregulation of eIF2B likely complements the A-site adjustments observed earlier, collectively optimizing translation efficiency to maintain cellular homeostasis. These findings highlight eIF2B as a pivotal regulator in sea rice HD961's adaptation to salt stress, ensuring the plant's resilience in saline environments by supporting robust protein synthesis under challenging conditions.

To explore eIF2B's role further, we examined the ribosome footprint distribution along its length. The distinct ribosome distribution observed (Fig. 6B) indicated that eIF2B's translation is regulated in response to salt stress. This unique ribosomal behavior suggests that eIF2B plays a role in adjusting the translation machinery to manage protein synthesis more efficiently during stress, contributing to HD961's high salt tolerance. Furthermore, the metagene analysis of P-site frequency revealed shifts in ribosome occupancy between control and salt-stressed conditions, further emphasizing the centrality of translation regulation in HD961's adaptation to salt stress (Fig. 6B). In addition to transcriptomic and ribosomal profiling, we observed the formation of eIF2B-containing bodies in salt-stressed rice (Fig. 6C). These bodies, highlighted by the yellow circles, suggest that eIF2B potentially undergoes phase separation under salt stress, forming condensates that may play a critical role in regulating translation and cellular stress responses. The distinct localization of eIF2B into these bodies under stress conditions further supports the idea that eIF2B is involved in compartmentalizing translation-related processes, which helps the plant adapt to the harsh salt stress environment. To confirm that eIF2B is upregulated at the protein level, we performed a Western Blot analysis, which validated our transcriptomic and ribosomal findings. The Western blot (Fig. 6D) confirmed the increased expression of eIF2B in salt-stressed HD961, supporting the hypothesis that eIF2B plays a critical role in salt stress adaptation by enhancing translation efficiency. Finally, to determine whether eIF2B regulation occurs primarily at the translational or transcriptional level, we compared its regulation at both the ribosomal and transcript levels (Additional file 2: Fig. S5A, B). The analysis revealed that eIF2B was significantly upregulated only at the ribosomal level, further confirming that eIF2B's function as a key regulator in HD961's adaptation to salt stress is driven by translational control rather than transcriptional regulation.

We next asked how salt stress remodels both transcript abundance and translational output in HD961. An examination of ribosome-protected footprints (Ribo-Seq) versus mRNA levels (RNA-Seq) shows that salt induces far fewer significant changes at the level of translation than at the level of transcription (Additional file 2: Fig. S5A, B). When we overlay pathway-specific gene sets on the Ribo-Seq volcano, only a handful of ion-transporter (blue), antioxidant (red-orange), and cell-wall (green) genes cross our significance thresholds (Additional file 2: Fig. S5C), indicating highly selective enhancement or repression of these functional classes.

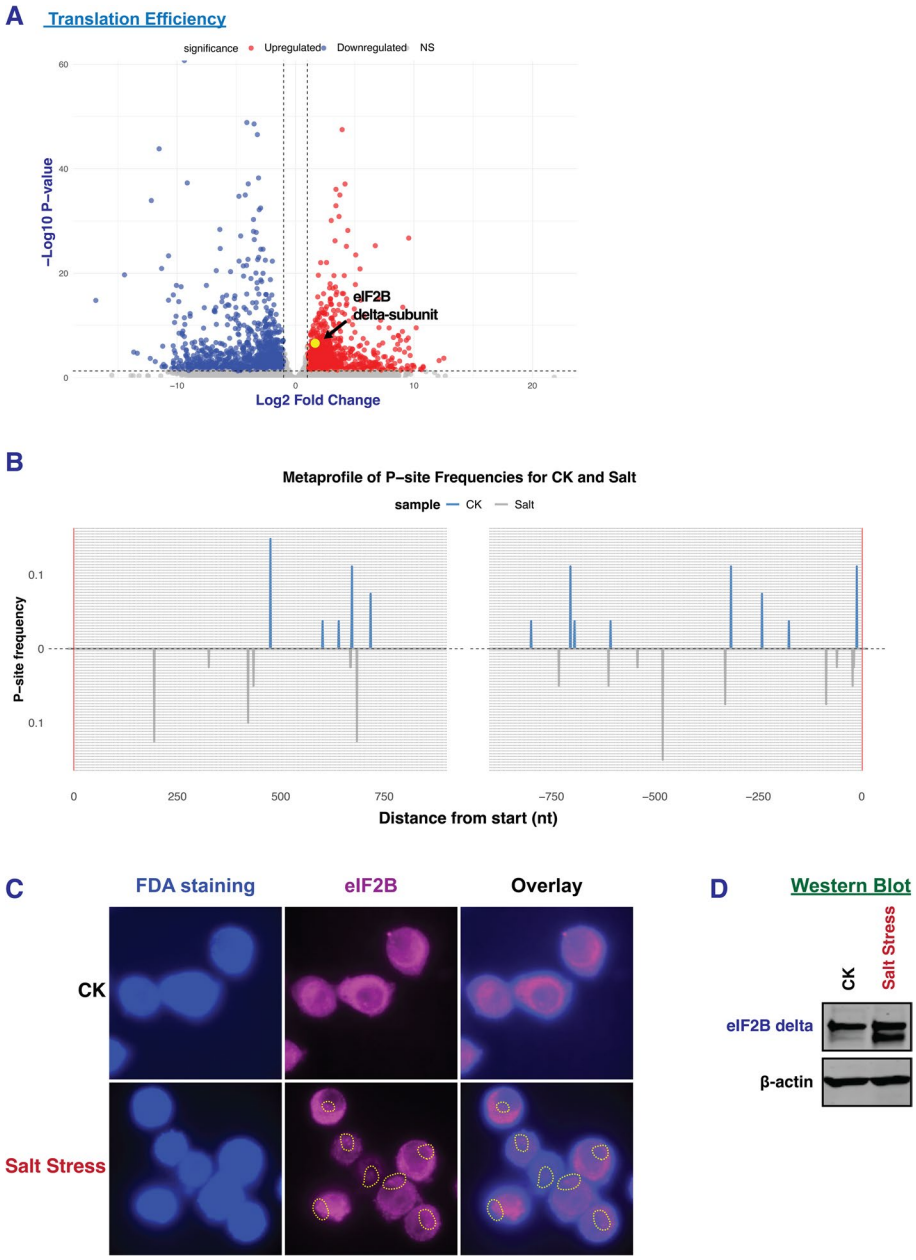

Fig. 6 Differential translation regulation and eIF2B dynamics in salt stress adaptation of sea rice HD961. **A** Volcano plot of translation efficiency. **B** Metagene analysis of eIF2B ribosome occupancy. **C** FDA viability staining and eIF2B immunofluorescence in HD961 protoplasts under control and salt stress, and **D** Western blot analysis. Statistical significance was defined as a false discovery rate (FDR)–adjusted *p* value below 0.05

Similarly, mapping TCA-cycle (green) and core metabolic (gold) genes onto the RNA-Seq volcano reveals that almost all TCA enzymes fall within the non-significant "grey zone" (Additional file 2: Fig. S5D), consistent with a broad down-tuning of central metabolism. To place these point-wise changes into a pathway context, we carried out KEGG and GO enrichment across all three data types (Additional file 2: Fig. S6). Ribo-Seq profiles are dominated by "Ribosome," "Spliceosome," and RNA-processing pathways (Additional file 2: Fig. S6A) and by ribonucleoprotein- and nuclear-complex components (Additional file 2: Fig. S6B). RNA-Seq enrichments shift toward hormone signaling, MAPK, and plant–pathogen interactions (Additional file 2: Fig. S6C) with cell-wall and vesicle components highlighted by GO-CC (Additional file 2: Fig. S6D). Finally, TE-upregulated genes are

specifically enriched for detoxification (phenylpropanoid, flavonoid, glutathione) and MAPK signaling (Additional file 2: Fig. S6E), and their cellular-component profile underscores secretory vesicles, Golgi, and cell-wall machinery (Additional file 2: Fig. S6F). Together, these data demonstrate that salt stress elicits a broad transcriptomic response but that HD961 directs its translational resources toward a narrow set of protective pathways while de-emphasizing growth-related metabolism.

Discussion

This study provides a comprehensive exploration of salt tolerance in sea rice HD961[36], leveraging a high-quality chromosome-level genome assembly alongside ribosome profiling (Ribo-seq) and RNA sequencing (RNA-seq) to uncover the critical role of translational regulation in stress adaptation. Our revised analysis presented a nuanced model of translational reprogramming in HD961. As shown in our volcano plots (Additional file 2: Fig. S5C), only a handful of canonical ion-transporter and antioxidant transcripts surpass the TE significance cutoffs under 150 mM NaCl, while KEGG enrichment of the TE-up cohort (Additional file 2: Fig. S6E) is dominated by secondary-metabolism pathways phenylpropanoid, flavonoid, glutathione biosynthesis, and stress-signaling cascades. Concurrently, GO-CC analysis (Additional file 2: Fig. S6F) highlights enrichment in vesicle/Golgi and cell-wall compartments rather than a wholesale shift in membrane transport machinery. These findings together suggest that, under salt stress, HD961 does not universally amplify translation of all ion-homeostasis genes; rather, it reallocates its translational resources toward detoxification and cell-wall remodeling processes that are most critical for maintaining cellular integrity and osmotic balance. This targeted reprogramming prioritizes detoxification and cell-wall remodeling rather than a broad enhancement of ion-homeostasis proteins, and is consistent with observations in other stress-tolerant species that similarly direct translational resources toward protective pathways [7, 9, 41–45]. By focusing translational resources on stress-responsive proteins, HD961 conserves energy while maximizing adaptive capacity—a hallmark of efficient stress resilience.

Our study identifies eukaryotic translation initiation factor 2B (eIF2B) as a key regulator of translational control under salt stress, offering novel insights into post-transcriptional mechanisms. Ribo-seq and Western blot analyses revealed significant upregulation of eIF2B at the translational and protein levels in HD961 under salt stress, with minimal changes at the transcriptional level (Fig. 6B–D, Additional file 2: Fig. S4B). This suggests that eIF2B's role is primarily modulated post-transcriptionally, optimizing protein synthesis during stress. Furthermore, immunofluorescence imaging showed the formation of eIF2B-containing bodies (Fig. 6C), potentially through phase separation—a mechanism increasingly linked to stress responses across species [46–53]. These bodies may compartmentalize translation-related processes, enhancing efficiency and coordination under salinity stress. As a critical factor in translation initiation and ribosome biogenesis [54–57], eIF2B emerges as a central player in HD961's adaptive strategy, orchestrating the translational machinery to meet the demands of saline environments.

Beyond eIF2B, our analysis of codon usage revealed targeted shifts in A-site occupancy under salt stress, rather than broad stalling (Fig. 5B). In the A-site scatter, most codons lie along the diagonal with unchanged decoding rates, while AAA shifts above the line (increased footprinting, slower decoding) and GCG shifts below (reduced footprinting, faster decoding). Consistent with this, our GCG-reporter shows higher luciferase activity under salt (Fig. 5D), indicating that accelerated decoding at GCG alleviates ribosome queuing and boosts translational throughput. Although these adjustments occur at specific codons, the overall stability of codon usage patterns highlights the robustness of HD961's translational machinery, which balances precise regulatory shifts with global translational fidelity during stress [45, 58]. Additionally, in our RNA-seq data, only a small subset of TCA-cycle genes were significantly downregulated under salt stress, like the NAD-dependent isocitrate dehydrogenase precursor, whereas the vast majority of core metabolic loci remained statistically unchanged (Additional file 2: Fig. S5D). Subsequent GO and KEGG enrichment analyses of those differentially expressed genes did not highlight the TCA cycle, but instead revealed modest activation of secondary metabolism (phenylpropanoid, flavonoid, glutathione pathways) and stress-signaling cascades (MAPK, plant–pathogen interaction) under saline conditions (Additional file 2: Fig. S6C-D). Together, these findings argue against a global suppression of primary metabolism; rather, HD961 appears to redirect metabolic flux toward protective and adaptive processes when challenged with high salt. This likely represents a strategic reallocation of resources, diverting energy from growth-related functions to stress defense mechanisms. Such metabolic reprogramming is a common adaptation in stress-tolerant plants, enabling them to sustain cellular integrity and survival under adverse conditions [45, 58–62]. In HD961, this shift supports the synthesis of proteins critical for ion homeostasis and oxidative stress mitigation, reinforcing its resilience in saline environments.

Our findings reveal a critical interplay between codon-specific ribosome stalling at the A site and the

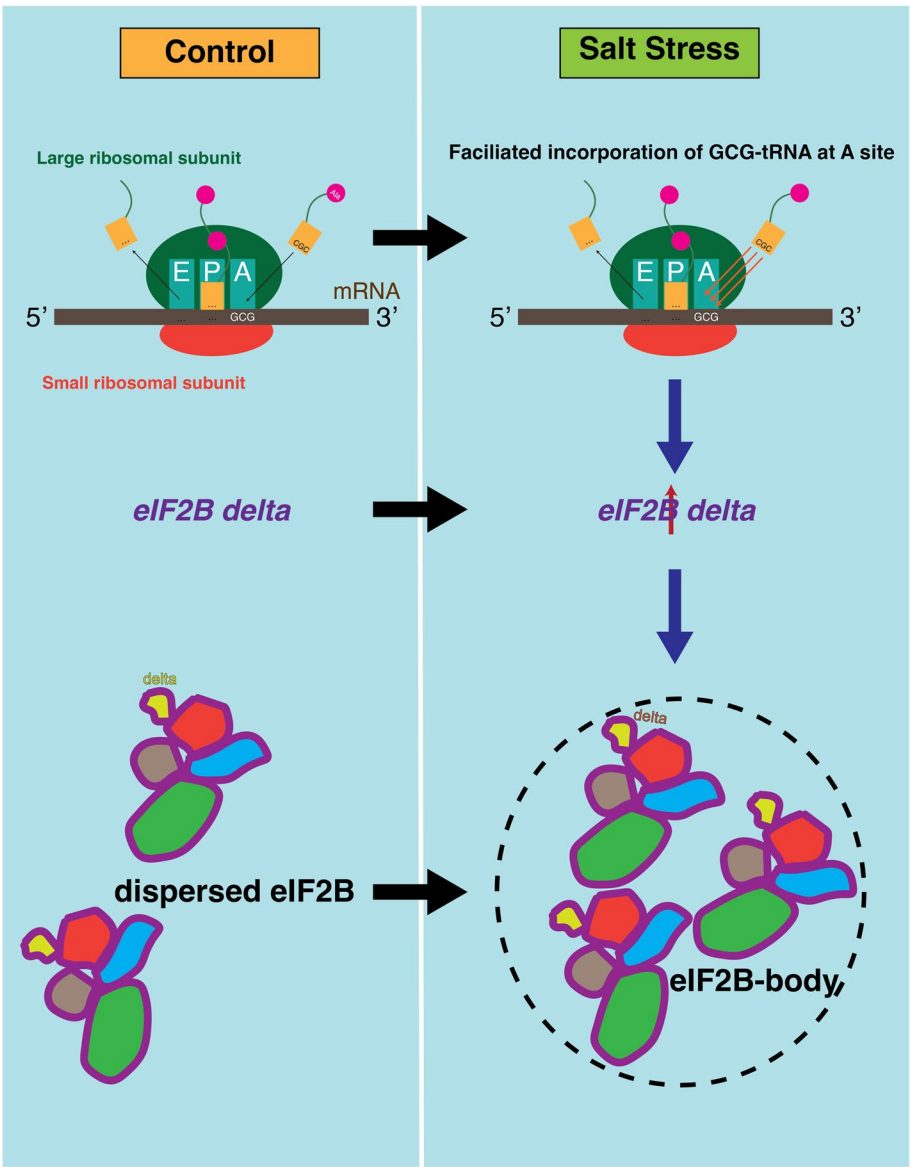

Fig. 7 Model of eIF2B modulation in salt-tolerant rice HD961 under salt stress

regulatory role of eIF2B in sea rice HD961's adaptation to salt stress, as illustrated in Fig. 7. Ribosome profiling identified significant stalling at the GCG codon (encoding alanine) under 150 mM NaCl stress, with reporter assays demonstrating increased translational signals for GCG-containing constructs, indicating reduced A-site occupancy (Fig. 5D). This stalling likely acts as a regulatory mechanism to prioritize the synthesis of stress-responsive proteins by temporarily slowing translation at specific codons, optimizing protein production under stress. Simultaneously, eIF2B, a key translation initiation factor, was significantly upregulated at the translational level and formed distinct eIF2B-containing bodies under salt stress, as confirmed by immunofluorescence (Fig. 6C). These bodies, potentially resulting from phase separation, may enhance translation efficiency by compartmentalizing eIF2B to support ribosome biogenesis and initiation [55, 56, 63, 64]. It suggests salt stress facilitates GCG-tRNA incorporation at the A site, correlating with the formation of eIF2B bodies, which could mitigate ribosome stalling by improving the availability of initiation factors, thereby ensuring efficient protein synthesis to maintain cellular homeostasis in saline environments (Fig. 7). Together, these findings indicate

that eIF2B's upregulation and spatial reorganization complement A-site stalling to fine-tune translational control, enabling HD961 to adapt effectively to salinity stress.

These findings have significant implications for breeding and biotechnological strategies aimed at enhancing salt tolerance in rice and other crops. The identification of eIF2B as a translational regulator highlights a promising target for genetic manipulation to boost stress resilience. Additionally, insights into codon-specific ribosome stalling and eIF2B-containing bodies open new research avenues for understanding translational control in plants. Future studies could explore the molecular pathways governing these processes, including the roles of RNA-binding proteins and other translation factors. Moreover, investigating how transposable elements—comprising over 35% of the HD961 genome (Table 4)—influence gene expression under stress could further elucidate the evolutionary underpinnings of its adaptability.

Conclusions

In summary, this study underscores the pivotal role of translational regulation in HD961's salt stress adaptation, integrating genomic and translatomic data to reveal how eIF2B and codon-specific mechanisms enhance resilience (Fig. 7). By combining advanced sequencing technologies with functional analyses, we provide a detailed view of the molecular strategies enabling HD961 to thrive in saline conditions, offering valuable resources for future efforts to improve abiotic stress tolerance in crops.

Methods

Plant material and growth conditions

Sea rice HD961 seeds were provided by the Guangdong Ocean University, Zhanjiang, China. Surface sterilization was carried out by immersing seeds in 70% ethanol for 5 min, followed by treatment with 10% sodium hypochlorite for 15 min, and subsequently rinsing with sterile distilled water. Germination was performed hydroponically in Murashige and Skoog (MS) medium at 28 °C with a 16-h light/8-h dark photoperiod and 60% relative humidity. After 14 days, seedlings were transferred into nutrient solutions containing either 0 mM NaCl (control) or 150 mM NaCl (salt stress). The seedlings were grown for an additional 48 h under these conditions. Tissues from roots and shoots were harvested, immediately frozen in liquid nitrogen, and stored at − 80 °C for subsequent genomic, transcriptomic, and translatomic analyses. Three biological replicates were maintained for each treatment condition to ensure the robustness of statistical analyses.

Genome sequencing and assembly

High-quality genomic DNA was extracted from 2-week-old HD961 seedlings using the cetyltrimethylammonium bromide (CTAB) method. For Nanopore sequencing, high-molecular-weight DNA (ranging from 20 to 80 kb) was prepared, and sequencing adapters were ligated to the DNA using the standard Nanopore protocol. Nanopore sequencing was carried out on the PromethION platform (Oxford Nanopore Technologies, Oxford, UK). The quality of raw reads was assessed using FastQC, followed by trimming of adapter sequences and removal of low-quality reads using Porechop (Oxford Nanopore Technologies). Additionally, Illumina short-read libraries with an insert size of approximately 350 bp were constructed and sequenced on the NovaSeq 6000 platform (Illumina, San Diego, CA, USA) to generate an additional ~ 150 Gb of data for the polishing process. The initial Nanopore reads were error-corrected using NECAT (v1.5.2) [65] and subjected to de novo assembly using SmartDenovo (v2.0.0) [66]. Following the initial assembly, the genome was polished through three rounds of Racon (v1.4.20) [67] and three rounds of Pilon (v1.23) [68] using the Illumina short reads. Hi-C libraries were constructed following the in situ Hi-C protocol (Rao et al., 2014). Sequencing was carried out on an Illumina NovaSeq 6000 platform (Illumina). High-quality Hi-C reads were processed using BWA (v0.7.17) [69], and the resulting uniquely mapped reads were used to scaffold the genome using LACHESIS (v1.0) [70]. The quality of the genome assembly was evaluated by aligning Illumina short reads to the final genome using BWA (v0.7.17). To assess the completeness of the genome, two complementary tools: CEGMA (Core Eukaryotic Genes Mapping Approach) [71] and BUSCO (Benchmarking Universal Single-Copy Orthologs) [72] were used.

Gene prediction and functional annotation

Gene prediction was carried out using a hybrid approach, integrating ab initio, homology-based, and RNA-seq-based predictions. For ab initio gene prediction, Augustus (v3.3) [73] and SNAP (v2013-02–21) [74] were used. For homology-based prediction, GeMoMa (v1.7.0) [75] was employed to align HD961 sequences to *Arabidopsis thaliana*, *Oryza sativa* Gramene, and IRGSP genomes. For transcript-based prediction, RNA-seq data were aligned to the genome using HISAT2 (v2.2.1) [76], and the alignments were assembled using StringTie (v1.3.5) [77]. Gene annotations were combined using Evidence Modeler (EVM) [78], resulting in a final set of 39,565 protein-coding genes. These genes were functionally annotated by aligning them to the following databases: NR, SwissProt, TrEMBL, Pfam, eggNOG, Gene Ontology

(GO), and KEGG, using BLASTp (v2.9.0). Noncoding RNAs (ncRNAs) were identified using specialized tools: tRNAs were predicted using tRNAscan-SE (v2.0) [79], rRNAs were identified with barrnap (v0.9), and miRNAs were detected using miRBase homology (v21) [80]. Additionally, small nucleolar RNAs (snoRNAs) and small nuclear RNAs (snRNAs) were predicted using Infernal (v1.1) with Rfam (v13) [81]. A total of 918 tRNAs, 464 rRNAs, and 195 miRNAs were identified. For pseudogene prediction, GenBlastA (v1.1) and GeneWise (v2.4.1) [82] were used.

Sample preparation and deep sequencing

Root samples of sea rice HD961 were treated with 150 mM NaCl to induce salt stress. For RNA sequencing (RNA-seq) and ribosome profiling (Ribo-seq), seedlings were grown hydroponically for 14 days, then transferred to either control conditions or salt stress conditions for an additional 48 h. Roots were harvested and immediately frozen in liquid nitrogen. For Ribo-seq, total RNA was extracted using the QEZ-seq protocol, and ribosome-protected fragments (RPFs) were isolated for deep sequencing.

Ribosome profiling

Ribo-seq libraries were constructed using the QEZ-seq protocol [29] from HD961 root tissues subjected to control and salt-stress conditions. Ribosome-protected fragments (RPFs) were extracted and sequenced on the Illumina NovaSeq 6000 platform (Illumina, San Diego, CA, USA). Data were processed using FastQC (Andrews, 2010) and trimmed using fastp [83] to remove adapter sequences and low-quality reads. Specifically, raw sequencing reads were first trimmed with fastp to remove adapter sequences, low-quality bases ($Q < 20$) and reads shorter than 25 nt or longer than 40 nt, thus recovering bona fide ribosome footprints and eliminating artifactual shorter fragments. Trimmed reads were then aligned with STAR to the HD961 genome assembly, using parameters optimized for short, end-to-end mapping and retaining only uniquely mapped reads ($MAPQ \geq 30$). PCR duplicates were marked and removed, and a parallel alignment against a curated rice rRNA reference confirmed > 90% rRNA depletion in each library. The resulting high-confidence RPF dataset was used to generate read-length distributions, metagene profiles around start and stop codons, and P-site assignments. RNA-seq and Ribo-seq data were integrated for translational efficiency (TE) analysis. TE was calculated as the ratio of ribosome occupancy to mRNA abundance, representing the efficiency of translation. Differential TE between control and salt-stressed conditions was determined using DESeq2 (v1.30.0) [84], applying a false discovery rate (FDR) threshold of < 0.05 and a fold-change cutoff of > 1.5. Codon usage bias and ribosome stalling were assessed using custom scripts in R (v4.0.2), and the resulting profiles were visualized using ggplot2 v3.3.3.

Reporter assay

In vitro translation assays were performed using crude plant lysates harvested from ribosome profiling experiments. The reporter genes used in this assay consisted of luciferase, preceded by either a poly(A) or poly(G) tract of varying lengths. The luciferase reporter DNA templates were synthesized by Integrated DNA Technologies (IDT) and included a T7 promoter, followed by a $(AAA)_5$ or $(GGG)_5$ sequence, and a poly(A) tail at the 3′ end. These constructs were used to assess translation efficiency in response to salt stress conditions. For each assay, 30 µL of the crude lysate was incubated with 0–10 µM of the respective reporter DNA template in a 50 µL translation buffer. The reaction mixtures were incubated at 25 °C for 10 min to allow translation to occur. The luciferase activity of the translation products was then measured using the Promega Luciferase Assay System (Promega, E1501). A 10 µL aliquot of the translation reaction was combined with 90 µL of the luciferase assay reagent, and the resulting luminescence was quantified immediately with a luminometer. Luciferase activity was normalized to total protein concentration, which was measured using the Bradford assay. Data were collected in triplicate for each template concentration, and the results are presented as the mean ± standard deviation (SD). Statistical significance was determined by performing a two-tailed Student's t test, with a significance threshold set at $p < 0.05$. All reporter assays were conducted to compare the translation efficiency of both the $(AAA)_5$ and $(GGG)_5$ reporter constructs under control (CK) and salt-stressed conditions.

Protoplast extraction and imaging

Protoplasts were isolated from root tissues of control (CK) and salt-stressed (150 mM NaCl, 48 h) HD961 seedlings by enzymatic digestion in 1.5% cellulase R10 and 0.5% macerozyme R10 (in 0.4 M mannitol, 20 mM MES, pH 5.7) for 3 h at 25 °C with gentle shaking, followed by filtration through 70 µm mesh and centrifugation at 100 × g for 5 min, as described before [17]. To assess viability, protoplasts were incubated with 5 µg/mL fluorescein diacetate (FDA) in the dark for 5 min, then washed once in W5 buffer. Then, cells were fixed in 4% (w/v) paraformaldehyde in PBS for 20 min at room temperature, washed three times in PBS, and permeabilized with 0.1% (v/v) Triton X-100 for 10 min. After blocking in 3% (w/v) BSA/PBS for 1 h, samples were incubated overnight at 4 °C with anti-eIF2B (sc-271332, Santa Cruz

Biotechnology) diluted 1:200 in 1% BSA/PBS, washed three times in PBS, and then stained for 1 h at room temperature with goat anti-mouse Alexa Fluor 568 (Invitrogen) diluted 1:500 in 1% BSA/PBS. Protoplasts were mounted on poly-L-lysine–coated slides and imaged on a confocal laser-scanning microscope (Zeiss LSM series) using identical acquisition settings for FDA (Ex 488 nm/Em 500–550 nm) and Alexa 568 (Ex 561 nm/Em 600–630 nm). All steps were performed with minimal light exposure to preserve fluorescence integrity.

Western blot analysis

For protein level confirmation, Western blotting was performed on total protein extracted from root tissues of HD961. Proteins were separated on SDS-PAGE gels, transferred to PVDF membranes, and incubated with the eIF2B antibody (sc-271332, Santa Cruz Biotechnology). Beta-actin (K800001M-HRP, Solarbio) was used as a loading control. The bound antibodies were detected using chemiluminescence according to the manufacturer's protocol.

Codon usage and ribosome stalling analysis

To investigate codon usage dynamics under salt stress, we employed a custom bioinformatics pipeline using R and Python. Ribosome-protected fragment (RPF) alignments were first filtered to remove low-quality reads and PCR duplicates. Next, we extracted the codon information at the E, P, and A sites using a 3-nt offset from the ribosome P-site. Codon usage frequencies were calculated separately for CK and salt-stressed samples. For ribosome stalling analysis, we identified positions in the coding sequences (CDSs) where ribosome density was significantly elevated above background levels, focusing on codons encoding Asn (AAU), Gln (CAA), and Glu (GAA). A sliding window approach was used to smooth the ribosome density profiles, and positions exhibiting a threefold or higher increase in ribosome occupancy were considered putative stalling sites. The significance of differences in codon usage between CK and salt-stressed samples was assessed using a Fisher's exact test ($p < 0.05$).

Metagene analysis

Metagene analysis was performed to examine the distribution of ribosome footprints around the start and stop codons. Reads corresponding to RPFs were aligned such that the P-site positions were set relative to the annotated start or stop codons. The frequency of ribosome occupancy at each position was then summed across all transcripts to generate a metagene profile. This approach enabled the comparison of ribosome occupancy between CK and salt-stressed conditions, highlighting changes in translation initiation, elongation, or termination under salt stress.

Bioinformatic visualization and statistical analyses

All data visualization (e.g., volcano plots, bar charts, heatmaps) was performed using R v4.0.2 packages such as ggplot2 v3.3.3 and ComplexHeatmap, or Python libraries such as matplotlib and seaborn. Unless otherwise specified, three biological replicates ($n = 3$) were used for each experimental condition, and statistical significance was determined by Student's t test or ANOVA with post-hoc tests ($p < 0.05$). GraphPad Prism or R was used for generating final plots and performing statistical analyses.

Abbreviations

TE	Translational efficiency (also used as "transposable elements" in genome sections; defined by context)
Ribo-seq	Ribosome profiling
RNA-seq	RNA sequencing
RPF	Ribosome-protected fragment
CDS	Coding sequence
UTR	Untranslated region
eIF2B	Eukaryotic translation initiation factor 2B
GO	Gene ontology
KEGG	Kyoto Encyclopedia of Genes and Genomes
BUSCO	Benchmarking Universal Single-Copy Orthologs
CEGMA	Core Eukaryotic Genes Mapping Approach
Hi-C	Chromosome conformation capture–based scaffolding
FDR	False discovery rate
ROS	Reactive oxygen species
SRA	Sequence Read Archive
MS	(Medium) Murashige and Skoog medium

Supplementary Information

The online version contains supplementary material available at https://doi.org/10.1186/s12915-025-02440-3.

Additional file 1: Tables S1–S3. Table S1-Summary of genome assembly statistics. Table S2-Overview of gene prediction methods and results. Table S3-Ribo-seq mapping statistics and rRNA depletion efficiency.

Additional file 2: Figures S1–S6. FigS1-Venn diagram of gene identification approaches and pathway analysis. FigS2-Quality assessment of ribosome-protected footprints mapped to the Nipponbare reference genome, including read length distribution, read extremity, P-site frequency, and sample correlations under control and salt stress conditions. FigS3-Ribosome P-site distribution in sea rice HD961 under control and salt stress, showing regional distribution, nucleotide composition comparisons, and start/stop codon heatmaps. FigS4-Codon usage analysis across coding sequences, including decile-based codon usage and GCG codon occupancy across translational efficiency categories. FigS5-Volcano plots of differential translation and transcription in HD961 under salt stress, highlighting ribosome occupancy, transcript abundance, and key functional gene categories. FigS6-Functional enrichment analyses of salt-responsive genes across Ribo-seq, RNA-seq, and translational efficiency datasets, with KEGG pathway and Gene Ontology term enrichment.

Additional file 3. The original images for Fig. 6C.

Additional file 4. The uncropped blots for Fig. 6D.

Acknowledgements
We thank all members of the Chen laboratory at Guangdong Ocean University for their technical support, insightful discussions, and assistance during this project.

Authors' contributions
The conceptualization of the study was led by MC. Nanopore and Illumina sequencing coordination, as well as Hi-C library construction and scaffolding, were carried out by MC and SY. Genome assembly, polishing, and annotation were also performed by MC and SY. Ribo-seq and RNA-seq data generation were handled by HC, MC and ZX, while data analysis was conducted by HC, MC and ZX. The manuscript writing was done by MC. Supervision was provided by MC, HZ, and YH. Funding acquisition was managed by MC and YH. All authors read, reviewed, and approved the final manuscript.

Funding
This work was financially supported by Guangdong Basic and Applied Basic Research Foundation (2024A1515110100), Research Startup Funding of Guangdong Ocean University (060302052103), the Special Project of Seed Industry Vitalization under Rural Revitalization Strategy in Guangdong Province (2022NPY00014), and the Natural Science Foundation of Guangdong Province (2024A1515012939).

Data availability
The processed datasets and analytical scripts are accessible upon request. Additionally, all sequencing data have been deposited to SRA (Sequence Read Archive) database (Project number: PRJNA1290000, [https://www.ncbi.nlm.nih.gov/bioproject/PRJNA1290000/](https:/www.ncbi.nlm.nih.gov/bioproject/PRJNA1290000)), ensuring that they are publicly available for further investigation by the scientific community. All of the R scripts and analysis pipelines used in this study have been deposited in a Zenodo archive (DOI: [https://doi.org/10.5281/zenodo.16632690](https:/doi.org/10.5281/zenodo.16632690)) and are publicly available for download.

Declarations

Ethics approval and consent to participate
Not applicable.

Consent for publication
Not applicable.

Competing interests
The authors declare no competing interests.

Received: 26 February 2025 Accepted: 9 October 2025
Published online: 03 November 2025

References

1. Wang Y, Huang L, Du F, Wang J, Zhao X, Li Z, et al. Comparative transcriptome and metabolome profiling reveal molecular mechanisms underlying *OsDRAP1*-mediated salt tolerance in rice. Sci Rep. 2021;11(1):5166.
2. Ma NL, Lam SD, Che Lah WA, Ahmad A, Rinklebe J, Sonne C, et al. Integration of environmental metabolomics and physiological approach for evaluation of saline pollution to rice plant. Environ Pollut. 2021;286:117214.
3. Lim H, Hwang H, Kim T, Kim S, Chung H, Lee D, Kim S, Park S, Cho W, Ji H et al: Transcriptomic analysis of rice plants overexpressing PsGAPDH in response to salinity stress. Genes (Basel) 2021, 12(5).
4. Froschel C, Komorek J, Attard A, Marsell A, Lopez-Arboleda WA, Le Berre J, et al. Plant roots employ cell-layer-specific programs to respond to pathogenic and beneficial microbes. Cell Host Microbe. 2021;29(2):299-310 e297.
5. Delseny M. Towards an accurate sequence of the rice genome. Curr Opin Plant Biol. 2003;6(2):101–5.
6. Mondal D, Kantamraju P, Jha S, Sundarrao GS, Bhowmik A, Chakdar H, et al. Evaluation of indigenous aromatic rice cultivars from sub-Himalayan Terai region of India for nutritional attributes and blast resistance. Sci Rep. 2021;11(1):4786.
7. Hasan MM, Rahman MA, Corpas FJ, Rahman MM, Jahan MS, Liu XD, et al. Salt stress tolerance in rice (*Oryza sativa* L.): a proteomic overview of recent advances and future prospects. Plant Stress. 2024;11:100307.
8. Muhammad M, Waheed A, Wahab A, Majeed M, Nazim M, Liu Y-H, et al. Soil salinity and drought tolerance: an evaluation of plant growth, productivity, microbial diversity, and amelioration strategies. Plant Stress. 2024;11:100319.
9. Shen X, Dai S, Chen M, Huang Y. Spermidine augments salt stress resilience in rice roots potentially by enhancing OsbZIP73's RNA binding capacity. BMC Plant Biol. 2024;24(1):786.
10. Sun S, Liu X, Zhang T, Yang H, Yu B. Functional characterisation of the transcription factor GsWRKY23 gene from Glycine soja in overexpressed soybean composite plants and Arabidopsis under salt stress. Plants (Basel). 2023;12(17):3030.
11. Li L, Zhu Z, Liu J, Zhang Y, Lu Y, Zhao J, et al. Transcription factor GmERF105 negatively regulates salt stress tolerance in Arabidopsis thaliana. Plants (Basel). 2023;12(16):3007.
12. Yan F, Zhang J, Li W, Ding Y, Zhong Q, Xu X, et al. Exogenous melatonin alleviates salt stress by improving leaf photosynthesis in rice seedlings. Plant Physiol Biochem. 2021;163:367–75.
13. Razzaq A, Ali A, Safdar LB, Zafar MM, Rui Y, Shakeel A, et al. Salt stress induces physiochemical alterations in rice grain composition and quality. J Food Sci. 2020;85(1):14–20.
14. Shelake RM, Kadam US, Kumar R, Pramanik D, Singh AK, Kim J-Y. Engineering drought and salinity tolerance traits in crops through CRISPR-mediated genome editing: targets, tools, challenges, and perspectives. Plant Commun. 2022;3(6):100417.
15. Reddy INBL, Kim B-K, Yoon I-S, Kim K-H, Kwon T-R. Salt tolerance in rice: focus on mechanisms and approaches. Rice Sci. 2017;24(3):123–44.
16. Ren G, Jiang Y, Li A, Yin M, Li M, Mu W, et al. The genome sequence provides insights into salt tolerance of *Achnatherum splendens* (Gramineae), a constructive species of alkaline grassland. Plant Biotechnol J. 2022;20(1):116–28.
17. Huang Y, Chen M, Chen D, Chen H, Xie Z, Dai S. Enhanced HSP70 binding to m6A-methylated RNAs facilitates cold stress adaptation in mango seedlings. BMC Plant Biol. 2024;24(1):1114.
18. Chen M, Dai S, Chen D, Zhu P, Feng N, Zheng D. Comparative analysis highlights uniconazole's efficacy in enhancing the cold stress tolerance of mung beans by targeting photosynthetic pathways. Plants. 2024;13(14):1885.
19. Alrajeh S, Naveed Khan M, Irhash Putra A, Al-ugaili DN, Alobaidi KH, Al Dossary O, et al. Mapping proteomic response to salinity stress tolerance in oil crops: towards enhanced plant resilience. J Genet Eng Biotechnol. 2024;22(4):100432.
20. Ingolia NT, Brar GA, Rouskin S, McGeachy AM, Weissman JS. The ribosome profiling strategy for monitoring translation in vivo by deep sequencing of ribosome-protected mRNA fragments. Nat Protoc. 2012;7(8):1534–50.
21. Ingolia NT, Lareau LF, Weissman JS. Ribosome profiling of mouse embryonic stem cells reveals the complexity and dynamics of mammalian proteomes. Cell. 2011;147(4):789–802.
22. Ingolia NT, Ghaemmaghami S, Newman JR, Weissman JS. Genome-wide analysis *in vivo* of translation with nucleotide resolution using ribosome profiling. Science. 2009;324(5924):218–23.
23. Chen M, Kumakura N, Saito H, Muller R, Nishimoto M, Mito M, et al. A parasitic fungus employs mutated eIF4A to survive on rocaglate-synthesizing *Aglaia* plants. Elife. 2023;12:e81302.
24. Chen M, Asanuma M, Takahashi M, Shichino Y, Mito M, Fujiwara K, et al. Dual targeting of DDX3 and eIF4A by the translation inhibitor rocaglamide A. Cell Chem Biol. 2021;28(4):475-486.e478.
25. Saito H, Handa Y, Chen M, Schneider-Poetsch T, Shichino Y, Takahashi M, et al. DMDA-Pata mediates RNA sequence-selective translation repression by anchoring eIF4A and DDX3 to GNG motifs. Nat Commun. 2024;15(1):7418.
26. Espinosa E, Bautista R, Larrosa R, Plata O. Advancements in long-read genome sequencing technologies and algorithms. Genomics. 2024;116(3):110842.

27. Satam H, Joshi K, Mangrolia U, Waghoo S, Zaidi G, Rawool S, et al. Next-generation sequencing technology: current trends and advancements. Biology (Basel). 2023;12(7):997.
28. Yamaguchi K, Kadota M, Nishimura O, Ohishi Y, Naito Y, Kuraku S. Technical considerations in Hi-C scaffolding and evaluation of chromosome-scale genome assemblies. Mol Ecol. 2021;30(23):5923–34.
29. Mao Y, Jia L, Dong L, Shu XE, Qian S-B. Start codon-associated ribosomal frameshifting mediates nutrient stress adaptation. Nat Struct Mol Biol. 2023;30(11):1816–25.
30. Son S, Park SR. Plant translational reprogramming for stress resilience. Front Plant Sci. 2023;2023:14.
31. Sackey OK, Feng N, Mohammed YZ, Dzou CF, Zheng D, Zhao L, et al. A comprehensive review on rice responses and tolerance to salt stress. Front Plant Sci. 2025;16:1561280.
32. Xu L, Zhang L, Liu Y, Sod B, Li M, Yang T, et al. Overexpression of the elongation factor MtEF1A1 promotes salt stress tolerance in *Arabidopsis thaliana* and *Medicago truncatula*. BMC Plant Biol. 2023;23(1):138.
33. Chen H, Xie Z, Chen M, Zhu P, Chen D, Huang Y, et al. Targeting eIF4A with RNA aptamers enhances salt stress tolerance in rice through modulation of translation initiation. Rice. 2025;18(1):62.
34. Huang Y, Chen H, Xie Z, Chen D, Chen M. Aptamer-mediated modulation of eEF1 enhances salt stress tolerance in rice. BMC Plant Biol. 2025;25(1):800.
35. Cui X, Cao Y, Lv M, Zhou S, Chen M, Li C, et al. The translation initiation factor eIF2 is phosphorylated to inhibit protein translation through reactive oxygen species under nutrient deficiencies in Arabidopsis. Stress Biol. 2025;5(1):7.
36. Yang S, Liu M, Chu N, Chen G, Wang P, Mo J, et al. Combined transcriptome and metabolome reveal glutathione metabolism plays a critical role in resistance to salinity in rice landraces HD961. Front Plant Sci. 2022;13:952595.
37. Fang X, Mo J, Zhou H, Shen X, Xie Y, Xu J, et al. Comparative transcriptome analysis of gene responses of salt-tolerant and salt-sensitive rice cultivars to salt stress. Sci Rep. 2023;13:1013.
38. Du H, Yu Y, Ma Y, Gao Q, Cao Y, Chen Z, et al. Sequencing and de novo assembly of a near complete indica rice genome. Nat Commun. 2017;8:15324.
39. Tanaka T, Nishijima R, Teramoto S, Kitomi Y, Hayashi T, Uga Y, et al. De novo genome assembly of the indica rice variety IR64 using linked-read sequencing and nanopore sequencing. G3 Genes|Genomes|Genetics. 2020;10(5):1495–501.
40. Shang L, He W, Wang T, Yang Y, Xu Q, Zhao X, et al. A complete assembly of the rice Nipponbare reference genome. Mol Plant. 2023;16(8):1232–6.
41. Zhou H, Shi H, Yang Y, Feng X, Chen X, Xiao F, et al. Insights into plant salt stress signaling and tolerance. J Genet Genomics. 2024;51(1):16–34.
42. Ullah MA, Abdullah-Zawawi M-R, Sukiran NL, Uddin MI, Ismail I, Zainal Z. In silico approach to investigate the potential HKT gene responsive to salt stress in rice. CABI Agric Biosci. 2024;5(1):49.
43. Han K, Zhao Y, Liu J, Tian Y, El-Kassaby YA, Qi Y, et al. Genome-wide investigation and analysis of NAC transcription factor family in *Populus tomentosa* and expression analysis under salt stress. Plant Biol (Stuttg). 2024;26(5):764–76.
44. Gao G, Yan L, Tong K, Yu H, Lu M, Wang L, et al. The potential and prospects of modified biochar for comprehensive management of salt-affected soils and plants: a critical review. Sci Total Environ. 2024;912:169618.
45. Chen M, Dai S, Chen D, Chen H, Feng N, Zheng D. Unveiling the translational dynamics of lychee (*Litchi chinesis* Sonn.) in response to cold stress. BMC Genomics. 2024;25(1):686.
46. Yuan S, Zhou G, Xu G. Translation machinery: the basis of translational control. J Genet Genomics. 2024;51(4):367–78.
47. Moon SL, Parker R. Analysis of eIF2B bodies and their relationships with stress granules and P-bodies. Sci Rep. 2018;8(1):12264.
48. Jiang Y, Peng X, Zhang Q, Liu Y, Li A, Cheng B, et al. Regulation of drought and salt tolerance by OsSKL2 and OsASR1 in rice. Rice. 2022;15(1):46.
49. Mishra S, Singh B, Panda K, Singh BP, Singh N, Misra P, et al. Association of SNP haplotypes of HKT family genes with salt tolerance in Indian wild rice germplasm. RICE. 2016;9:15.
50. Tu Y, Jiang AM, Gan L, Hossain M, Zhang JM, Peng B, et al. Genome duplication improves rice root resistance to salt stress. RICE. 2014;7:15.
51. Sahoo RK, Ansari MW, Tuteja R, Tuteja N. OsSUV3 transgenic rice maintains higher endogenous levels of plant hormones that mitigates adverse effects of salinity and sustains crop productivity. RICE. 2014;7:17.
52. Hairmansis A, Berger B, Tester M, Roy SJ. Image-based phenotyping for non-destructive screening of different salinity tolerance traits in rice. RICE. 2014;7:16.
53. Kumar K, Kumar M, Kim SR, Ryu H, Cho YG. Insights into genomics of salt stress response in rice. RICE. 2013;6:27.
54 Tsai JC, Miller-Vedam LE, Anand AA, Jaishankar P, Nguyen HC, Renslo AR, et al. Structure of the nucleotide exchange factor eIF2B reveals mechanism of memory-enhancing molecule. Science. 2018;359(6383):0939.
55. Hanson FM, Hodgson RE, de Oliveira MIR, Allen KE, Campbell SG. Regulation and function of eIF2B in neurological and metabolic disorders. Biosci Rep. 2022;42(6):BSR20211699.
56. Kashiwagi K, Yokoyama T, Nishimoto M, Takahashi M, Sakamoto A, Yonemochi M, et al. Structural basis for eIF2B inhibition in integrated stress response. Science. 2019;364(6439):495–9.
57. Bogorad AM, Lin KY, Marintchev A. eIF2B mechanisms of action and regulation: a thermodynamic view. Biochemistry. 2018;57(9):1426–35.
58. Kim EY, Wang L, Lei Z, Li H, Fan W, Cho J. Ribosome stalling and SGS3 phase separation prime the epigenetic silencing of transposons. Nat Plants. 2021;7(3):303–9.
59. Snieckute G, Genzor AV, Vind AC, Ryder L, Stoneley M, Chamois S, et al. Ribosome stalling is a signal for metabolic regulation by the ribotoxic stress response. Cell Metab. 2022;34(12):2036-2046 e2038.
60. Yang X, Song B, Cui J, Wang L, Wang S, Luo L, et al. Comparative ribosome profiling reveals distinct translational landscapes of salt-sensitive and -tolerant rice. BMC Genomics. 2021;22(1):612.
61. Rubio A, Ghosh S, Mulleder M, Ralser M, Mata J. Ribosome profiling reveals ribosome stalling on tryptophan codons and ribosome queuing upon oxidative stress in fission yeast. Nucleic Acids Res. 2021;49(1):383–99.
62. Iwakawa HO, Lam AYW, Mine A, Fujita T, Kiyokawa K, Yoshikawa M, et al. Ribosome stalling caused by the Argonaute-microRNA-SGS3 complex regulates the production of secondary siRNAs in plants. Cell Rep. 2021;35(13):109300.
63. Basu I, Gorai B, Chandran T, Maiti PK, Hussain T. Selection of start codon during mRNA scanning in eukaryotic translation initiation. Commun Biol. 2022;5(1):587.
64. Castellano MM, Merchante C. Peculiarities of the regulation of translation initiation in plants. Curr Opin Plant Biol. 2021;63:102073.
65. Chen Y, Nie F, Xie SQ, Zheng YF, Dai Q, Bray T, et al. Efficient assembly of nanopore reads via highly accurate and intact error correction. Nat Commun. 2021;12(1):60.
66. Liu H, Wu S, Li A, Ruan J. Smartdenovo: a de novo assembler using long noisy reads. GigaByte. 2021;2021:gigabyte15.
67. Vaser R, Sović I, Nagarajan N, Šikić M. Fast and accurate de novo genome assembly from long uncorrected reads. Genome Res. 2017;27(5):737–46.
68. Walker BJ, Abeel T, Shea T, Priest M, Abouelliel A, Sakthikumar S, et al. Pilon: an integrated tool for comprehensive microbial variant detection and genome assembly improvement. PLoS ONE. 2014;9(11):e112963.
69. Li H, Durbin R. Fast and accurate short read alignment with Burrows-Wheeler transform. Bioinformatics. 2009;25(14):1754–60.
70. Burton JN, Adey A, Patwardhan RP, Qiu R, Kitzman JO, Shendure J. Chromosome-scale scaffolding of de novo genome assemblies based on chromatin interactions. Nat Biotechnol. 2013;31(12):1119–25.
71. Parra G, Bradnam K, Korf I. CEGMA: a pipeline to accurately annotate core genes in eukaryotic genomes. Bioinformatics. 2007;23(9):1061–7.
72. Simão FA, Waterhouse RM, Ioannidis P, Kriventseva EV, Zdobnov EM. BUSCO: assessing genome assembly and annotation completeness with single-copy orthologs. Bioinformatics. 2015;31(19):3210–2.
73. Keller O, Kollmar M, Stanke M, Waack S. A novel hybrid gene prediction method employing protein multiple sequence alignments. Bioinformatics. 2011;27(6):757–63.
74. Korf I. Gene finding in novel genomes. BMC Bioinformatics. 2004;5(1):59.
75. Keilwagen J, Hartung F, Grau J. GeMoMa: homology-based gene prediction utilizing intron position conservation and RNA-seq data. Methods Mol Biol. 2019;1962:161–77.
76. Kim D, Paggi JM, Park C, Bennett C, Salzberg SL. Graph-based genome alignment and genotyping with HISAT2 and HISAT-genotype. Nat Biotechnol. 2019;37(8):907–15.

77. Shumate A, Wong B, Pertea G, Pertea M. Improved transcriptome assembly using a hybrid of long and short reads with StringTie. PLoS Comput Biol. 2022;18(6):e1009730.
78. Haas BJ, Salzberg SL, Zhu W, Pertea M, Allen JE, Orvis J, et al. Automated eukaryotic gene structure annotation using EVidenceModeler and the program to assemble spliced alignments. Genome Biol. 2008;9(1):R7.
79. Lowe TM, Eddy SR. tRNAscan-SE: a program for improved detection of transfer RNA genes in genomic sequence. Nucleic Acids Res. 1997;25(5):955–64.
80. Kozomara A, Birgaoanu M, Griffiths-Jones S. MiRBase: from microrna sequences to function. Nucleic Acids Res. 2018;47(D1):D155–62.
81. Griffiths-Jones S, Bateman A, Marshall M, Khanna A, Eddy SR. Rfam: an RNA family database. Nucleic Acids Res. 2003;31(1):439–41.
82. Zhao H, Wang W, Yang Y, Wang Z, Sun J, Yuan K, et al. A high-quality chromosome-level wild rice genome of *Oryza coarctata*. Sci Data. 2023;10(1):701.
83. Chen S, Zhou Y, Chen Y, Gu J. Fastp: an ultra-fast all-in-one FASTQ preprocessor. Bioinformatics. 2018;34(17):i884–90.
84. Love MI, Huber W, Anders S. Moderated estimation of fold change and dispersion for RNA-seq data with DESeq2. Genome Biol. 2014;15(12):550.

Publisher's Note